Modeling the human limb skeletal development using human pluripotent stem cell-derived skeletal assembloid

Tomoka Takao[1], Tatsunori Osone[1], Kohei Sato[1,2], Daisuke Yamada[1], Yuki Fujisawa[1], Masaya Hagiwara[3], Eiji Nakata[2], Toshifumi Ozaki[2], Junya Toguchida[4], Takeshi Takarada[1,*]

[1]Department of Regenerative Science, Okayama University Graduate School of Medicine, Dentistry and Pharmaceutical Sciences, Okayama, Japan.
[2]Department Orthopedic Surgery, Okayama University Graduate School of Medicine, Dentistry and Pharmaceutical Sciences, Okayama, Japan.
[3]Cluster for Pioneering Research, RIKEN, Saitama, 351-0198, Japan.
[4]Department of Cell Growth and Differentiation, Center for iPS Cell Research and Application, Kyoto University, Kyoto, Japan.

*Corresponding author, takarada@okayama-u.ac.jp

SUMMARY

Despite recent advances in pluripotent stem cell-based approaches inducing the skeletal cells, recapitulating human limb skeletal development in terms of structure and longitudinally oriented growth remains an unresolved challenge. Here, we report a method to differentiate human pluripotent stem cells into region-specific skeletal organoids harboring the interzone/articular chondrocyte progenitors (IZ/ACP) and growth plate chondrocytes (GPC), via PRRX1^{+} limb-bud mesenchymal cells. Comparative analysis demonstrated marked similarities of IZ/ACP and GPC organoid to the human embryonic limb, further characterized with *in vivo* graft fate and regenerative capacity. We also mimicked the limb skeletal developmental process in a spatially structured manner by vertically positioning two IZ/ACP organoids at both ends of a GPC organoid, namely human skeletal assembloid. Notably, human skeletal assembloid recapitulated an endochondral ossification with a longitudinal skeletal growth upon transplantation. In sum, our study provides a novel research platform for human limb skeletal development and disease.

Keywords
Human pluripotent stem cells, organoid, assembloid, skeletal development, endochondral ossification

INTRODUCTION

Understanding the human skeletal development is essential not only for advancing bone physiology, such as providing a weight-bearing framework, regulating endocrine functions, and supporting hematopoiesis [1], but also for addressing clinical challenges, including osteoarthritis [2,3], nonunion fractures [4] in the elderly, and congenital skeletal disorders [5], which remain unresolved by conventional therapies. Although ethical constraints on research into human skeletal development have long existed, advancements in human pluripotent stem cells (hPSCs) have transformed the field. With their self-renewal and pluripotency, hPSCs allow to provide experimental models that mimic skeletal development by navigating the brachiating landscape and efficiently differentiating intermediate stem/progenitor cells into desired cell types for regenerative medicine and recapitulation of congenital skeletal disorders [6]. In mammals, the skeleton is derived from three distinct embryonic sources according to the anatomical region. The axial skeleton (for examples, vertebrae and rib) is specified from the paraxial mesoderm, cranial skeleton (for example, facial and cranial bone), whereas the appendicular skeleton (for example, limb) arises from the lateral plate mesoderm (LPM) [7]. Moreover, ossification during the skeletal development is mediated by two distinct processes: intramembranous ossification and endochondral ossification. In intramembranous ossification, mesenchymal cells are directly differentiated into osteoblasts that are responsible for bone formation [8]. Conversely, in endochondral ossification, a cartilaginous template (anlagen) is initially established, which is subsequently replaced to the bone [9]. Recent studies have employed hPSCs to recapitulate skeletal lineages, successfully inducing skeletal cells or organoids (three-dimensional structures grown from stem cells that mimic certain aspects of organs) that participate in intramembranous ossification [10–14] or endochondral ossification [15–21]. However, replicating processes that emulate skeletal morphology with skeletal growth through human pluripotent stem cells remains an unresolved challenge.

The development of limb skeletal structures is initiated by condensation of PRRX1$^+$ limb-bud mesenchymal (LBM) cells, followed by the formation of skeletal anlagen composed of immature chondrocytes [22]. The joint interzone develops at the position of the presumptive joint and precedes articular cartilage differentiation and joint cavitation. Immature chondrocytes outside the interzone undergo hypertrophy at the mid-diaphysis as the first step of endochondral ossification [22]. Vasculature invades hypertrophic chondrocytes and subsequently forms the bone marrow cavity and growth plate chondrocyte/cartilage, which support the longitudinal skeletal growth of the limbs until puberty [9,22] (Figures 1A and 3A). To replicate these complex human limb developmental processes, the induction of LBM cells from hPSCs is essential. Recently, we successfully generated PRRX1$^+$ LBM cells from hPSCs in a stable and scalable manner by

employing a PRRX1-tdTomato reporter hPSCs [23,24]. This achievement has laid the foundation for the induction of intermediate structures, such as the interzone and growth plate cartilage, from hPSCs. In this study, we developed a protocol to generate distinct intermediate organoids, each characterized as interzone/articular chondrocyte progenitors (IZ/ACP) or growth plate chondrocytes (GPC), from ontogenetically defined PRRX1$^+$ LBM cells derived from hPSCs, through the establishment of lineage-specific tdTomato reporter PSC lines. Additionally, by employing a three-dimensional assembly strategy for these intermediate tissue constructs, we successfully recapitulated the spatial developmental processes, thereby reproducing skeletal growth along the longitudinal axis.

RESULTS

Generation of ontogenetically-defined IZ/ACP and GPC organoids from hPSCs

In our previous study, we demonstrated the induction and expansion of PRRX1$^+$ limb-bud-like mesenchymal cells (expandable limb-bud-like mesenchymal cells, ExpLBM cells) from human pluripotent stem cells [23]. This protocol begins with differentiation into the mid-primitive streak and LPM, followed by the induction of LBM cells, which have chondrogenic capacity in the presence of BMP4, TGFβ1, and GDF5 (Figure S1A). The expression levels of each marker gene (pluripotent markers, LPM markers, LBM markers, and chondrocyte markers) clearly revealed the sequential induction of genes representative of each differentiation stage (Figure S1B). Chromatin accessibility, epigenetically regulated by histone modifications such as acetylation and methylation, determines the access of transcription factors and underlies cell-type-specific gene expression [25,26]. Therefore, we investigated cell specificity during the stepwise induction protocol by analyzing chromatin accessibility using ATAC-seq and histone modifications using CUT&Tag. *NANOG, HAND1*, and *PRRX1* are cell-specific markers for pluripotent cells, LPM, and LBM cells, respectively, and the mRNA expression of these genes was found to be specific to each developmental stage. When the 5' flanking regions of these genes were analyzed using ATAC-seq and CUT&Tag with antibodies against H3K27Ac and H3K27me3, peaks of ATAC-seq and H3K27Ac were observed at time points corresponding to the mRNA expression peaks. In contrast, the H3K27me3 peaks showed an inverse correlation with these patterns (Figure S1C). Furthermore, we assessed whether our ontogenetically-defined induction protocol for ExpLBM cells recapitulates the formation of either forelimb or hindlimb. Reanalysis of single-cell RNA-seq data of human forelimb buds and hindlimb buds [27] revealed that TBX5 was highly expressed in forelimb buds, while *PITX1* and *ISL1* were enriched in hindlimb buds, consistent with previous mouse studies [28] (Figure S1D). We found that stepwise induction processes from hPSCs to ExpLBM cells exclusively showed *PITX1* and *ISL1* expression, but not *TBX5* expression (Figure

S1D). Under these conditions, high peak patterns of ATAC-seq and H3K27Ac were found in *ISL1* and *PITX1*, but not in *TBX5*. On the other hand, H3K27me3 peaks were found in *TBX5*, but not in *ISL1* and *PITX1* (Figure S1E). These results indicate that our induction protocols generate ontogenetically-defined LBM cells that recapitulate hindlimb bud initiation.

Limb skeletal development begins with the condensation of LBM cells, forming a cartilage template. This template subsequently differentiates into two distinct lineages: articular permanent cartilage, which develops through intermediate GDF5-expressing interzone cells, and growth plate cartilage comprising resting, proliferative, and SP7-expressing hypertrophic chondrocytes, which drives longitudinal bone growth. Previous our studies have enabled the generation of cartilage tissues from ExpLBM cells by 30 ng/ml BMP4 and 10 ng/ml TGFβ1 supplementation *in vitro* [23,24]. However, RNA-seq analysis of cartilage generated using this protocol revealed the expression of markers for both interzone/articular cartilage and growth plate cartilage (Figure S1B). In addition, subcutaneous transplantation of this cartilage into NOD-SCID mice revealed that some of the transplanted cartilages maintained hyaline cartilaginous-like tissues, but some showed an ossification with columnar chondrocytes and spongy bone at 8 weeks (Figure S1F). Thus, previous our chondrogenic induction protocol from ExpLBM cells does not seem to selectively induce each lineage for interzone/articular cartilage or growth plate cartilage. In order to develop a lineage-selective induction protocol of ExpLBM cells into interzone/articular cartilage or growth plate cartilage, we established GDF5-tdTomato reporter iPSCs (GDF5$^{3'tdTomato}$ hiPSCs) and SP7-tdTomato reporter hESCs (SP7$^{3'tdTomato}$ hESCs) for visualizing a GDF5 (interzone marker)-positive or SP7 (hypertrophic chondrocyte marker)-positive cells. hPSCs were electroporated with the targeting vector harboring a homology arm and IRES-tdTomato-PGK-Neo cassette, and the PX459-gRNA genome editing vector. Electroporated cells were selected with puromycin and G418, followed by cell cloning to isolate 3'tdTomato-reporter PSCs. Single colonies were expanded, and genomic DNA was extracted to identify correct insertion of the knock-in reporter cassette. PCR results showed that the selected clone harbored a homozygous knock-in reporter cassette (Figure S2A). These reporter clones of GDF5$^{3'tdTomato}$ hiPSCs or SP7$^{3'tdTomato}$ hESCs were therefore chosen for the induction experiments.

Next, ExpLBM cells derived from GDF5$^{3'tdTomato}$ hiPSCs or SP7$^{3'tdTomato}$ hESCs were condensed into aggregates (step 1) and subsequently differentiated into chondrocytes using BMP4, TGFβ1, and FGF2 (step 2). This was followed by treatment with 21 different combinations of chemicals in the presence of 30 ng/ml BMP4, 10 ng/ml TGFβ1 and 10 ng/ml GDF5 for 14 days (Figure 1A). Among the different combinations tested, we found that the addition of PD0325901 (a MEK inhibitor) in the presence of BMP4 and TGFβ1 was necessary to induce GDF5-tdTomato expression. In contrast, high concentrations of BMP4 and TGFβ1 (300 ng/mL BMP4 and 100 ng/mL TGFβ1) effectively induced SP7-tdTomato expression (Figure 1B and S2B). Principal

component analysis revealed distinct differential gene expression profiles across pluripotent cells (day 0), LPM cells (day 2), LBM cells (day 4), ExpLBM cells, and cell aggregates treated with 30 ng/mL BMP4 and 10 ng/mL TGFβ1 (conventional), 30 ng/mL BMP4, 10 ng/mL TGFβ1, and PD0325901 (hereafter referred to as the IZ/ACP organoid strategy), or 300 ng/mL BMP4 and 100 ng/mL TGFβ1 (hereafter referred to as the GPC organoid strategy) (Figure 1C). Notably, RNA-seq analysis clearly demonstrated that interzone/articular cartilage markers (e.g., *GDF5, PRG4, BARX1*) were enriched in the IZ/ACP organoid, whereas growth plate cartilage markers (e.g., *RUNX2, SP7, IHH, COL10A1*) were highly expressed in the GPC organoid (Figure 1D). We next assessed the expression patterns of each markers by immunohistochemistry in ExpLBM cell aggregates, IZ/ACP and GPC organoids. While SOX9 and ACAN were consistently expressed in all tested aggregates, PRG4 and COL1 were detected exclusively in IZ/ACP organoid. In contrast, RUNX2, COLX, and SP7 were observed only in GPC organoid (Figure 1E). We also confirmed that 2 different hPSCs (802-3G hiPSCs and SEES4 hESCs) could established similar expression profile by RT-qPCR analysis (Figure S2C).

To further analyze lineage specification and its heterogeneity, we performed single-cell RNA sequencing (scRNA-seq) on 9741 cells from ExpLBM, 5090 cells from IZ/ACP organoid, and 4660 cells from GPC organoid. Uniform manifold approximation and projection (UMAP) dimensionality identified 2 clusters in ExpLBM cells [LBM cells (non-dividing) and MKI67+ limb-bud mesenchymal cells (dividing)], 2 clusters in IZ/ACP organoid (GDF5-positive interzone cells and PRG4-positive articular chondrocyte progenitor) and 2 clusters in GPC organoid (IHH-positive pre-hypertrophic chondrocytes and SP7-positive hypertrophic chondrocytes), based on gene expression patterns (Figures 1F, 1G and S3A). To evaluate the similarity between these hPSC-derived cells and cells from the human embryo, we integrated their scRNA-seq expression profiles with data from the human limb developmental process [27]. Our analysis revealed that ExpLBM cells, IZ/ACP, and GPC organoids most closely resemble limb-bud mesenchyme (LimbMes1), articular chondrocytes, and hypertrophic chondrocytes observed during human limb development, respectively (Figure 1H). Dot plots from scRNA-seq analyses of ExpLBM cells, IZ/ACP, and GPC organoids confirmed their identities as limb-bud mesenchyme, interzone and articular chondrocytes, and hypertrophic chondrocytes, respectively, by comparing the expression of cell-type-specific genes in each cluster to those observed in scRNA-seq analyses of human embryonic limb cells (Figure 1I). Furthermore, KEGG pathway enrichment analysis was performed on genes exhibiting significant differential expression identified through pseudotime trajectory analysis using scRNA-seq datasets of human embryonic limbs, with LimbMes1 designated as the initial state. This analysis revealed that, unlike differentiation into growth plate chondrocytes, the developmental transition from LBM cells to articular chondrocytes was characterized by suppression of MAPK signaling (Figures S3B and S3C). These findings indicate

that our differentiation strategy from hPSCs into two distinct chondrocyte lineage including IZ/ACP and GPC organoids recapitulate the human skeletal developmental process of hindlimb-bud.

Assessment of IZ/ACP and GPC organoids on graft fate and regenerative capacity

Next, we investigated the graft fate by subcutaneously transplanting these organoids into NOD-SCID mice. Transplanted IZ/ACP organoids remained Safranin-O positive hyaline cartilaginous-like tissues without ossification up to 3 months post-transplantation, whereas transplanted GPC organoids exhibited ossification, including the presence of columnar chondrocytes and spongy bone formation observed at 3 months (Figure 2A). Furthermore, the cells of mouse articular cartilage exhibit smooth surfaces, as observed via scanning electron microscopy (SEM), and possess simple intracellular organelle structures, as seen through transmission electron microscopy (TEM). This phenotype closely resembled that of transplanted IZ/ACP organoid-derived cartilaginous tissues. In contrast, the cells of mouse growth plate cartilage are characterized by an abundance of cellular projections (SEM) and are rich in rough endoplasmic reticulum and Golgi apparatus (TEM). This appearance was strikingly similar to that of transplanted GPC organoid-derived cartilaginous tissues (Figure 2B). Indeed, immunohistochemical analysis revealed that transplanted IZ/ACP organoid-derived cartilaginous tissues were positively stained for COLII and ACAN but did not express pre-/hypertrophic chondrocyte markers, such as RUNX2 and SP7, nor the macrophage marker CD107b (LAMP2) or the endothelial cell marker endomucin (EMCN). In contrast, transplanted GPC organoid-derived cartilaginous tissues expressed not only COLII and ACAN but also RUNX2 and SP7, and contained cells positive for CD107b and EMCN (Figure 2C).

To demonstrate regenerative efficacy of IZ/ACP organoid *in vivo*, these ExpLBM-derived IZ/ACP organoids were transplanted into osteochondral defects created in the knee joint articular cartilage of X-linked severe combined immunodeficiency (SCID) rats. At 1 or 3 months after transplantation, IZ/ACP organoids were successfully engrafted into osteochondral defects, as evidenced by human vimentin (hVIMENTIN) expression. These organoids produced extracellular matrix (ECM) that was positive for Safranin O staining and immunohistochemistry for COL2 and ACAN. Notably, PRG4, a marker of the superficial zone of articular cartilage, was specifically expressed in the joint-side surface of the graft (Figure 2D). During fracture healing, the cartilaginous callus formed at the injury site undergoes endochondral ossification, facilitating bone repair [29]. To evaluate the regenerative capacity of GPC organoid, we transplanted them into critical-sized femur defects in SCID rats. Periodic observation of mineralized bone using μCT revealed that, in the absence of transplantation, no bone union occurred, resulting in a condition resembling nonunion. In contrast, transplantation of GPC organoids led to bone formation at the defect site, observed by day 28 post-transplantation, with complete bone union achieved by day

56 (Figure 2E). Histological analysis further confirmed active bone formation at the transplantation site, with remnants of Safranin O-stained hyaline cartilaginous-like matrix (Figure 2F). Human-specific nucleoli staining demonstrated that the newly formed bone was predominantly graft-derived (Figure 2G). Finally, bone strength at the fracture site was assessed 3 months post-transplantation using a three-point bending test. Although the values did not reach those of intact femurs without defects, significant recovery in ultimate stress (N) and extrinsic stiffness (N/mm²) was observed in GPC organoid-transplanted femurs (Figure 2H). Collectively, these results demonstrate that IZ/ACP organoids exhibit characteristics of interzone/articular chondrocyte progenitors, which generate articular permanent cartilage, whereas GPC organoids display characteristics of growth plate chondrocytes, driving endochondral ossification.

Generation of skeletal assembloid with IZ/ACP and GPC organoid to recapitulate human limb skeletal development.

In the early stages of skeletal formation, the process begins with the condensation of LBM cells, leading to the formation of the cartilage anlagen. Subsequently, this structure develops into an in which the growth plate chondrocyte, contributing to the elongation of the bone along its longitudinal axis through endochondral ossification, is flanked by the interzone, the region that will eventually give rise to future joints (Figure 3A) [22]. The generation of two types of organoids, harboring characteristics of interzone/articular chondrocyte progenitors or growth plate chondrocytes, enabled the reconstruction of this skeletal complex in vitro. To this end, we fused IZ/ACP organoids and GPC organoids to produce a skeletal assembloid. To facilitate visualization, we inserted a ubiquitous GFP or Kusabira Orange (KuO) marker into hiPSCs using a piggyBac transposon system, followed by the generation of IZ/ACP or GPC organoids, respectively (Figure 3B). Two GFP-labeled IZ/ACP organoids were positioned vertically at both ends of a KuO-labeled GPC organoids within low-melting point agarose gel. By day 7, the three organoids had fused within the wells (Figure 3C), forming a skeletal complex, which was subsequently transplanted subcutaneously into NOD-SCID mice. At 1 and 6 months post-transplantation, the excised tissues retained the expression of GFP and KuO (Figure 3D). Notably, significant longitudinal growth of the skeletal assembloid was observed over time post-transplantation (Figure 3E). Furthermore, μCT analysis at 6 months post-transplantation revealed ossification in the central region (Figure 3F). Histological analysis of transplanted skeletal assembloid at 1 month demonstrated that the *GFP*-positive regions were observed at the peripheral edges of the tissue, while KuO-positive regions were localized in the central area. COL2 was detected throughout the entire tissue, whereas PRG4 was predominantly observed in the peripheral regions. COLX and SP7 were detected in the KuO-positive central region of the tissue. In contrast, no expression of CTSK or EMCN was observed (Figure 3F). At 6 months post-transplantation, the *GFP*-positive regions

remained localized at the peripheral edges of the transplanted tissue, as observed at 1 month post-transplantation. These regions were positive for Safranin O, COL2, and PRG4. Meanwhile, in the KuO-positive regions at six months, a columnar structure characteristic of growth plate cartilage, positive for COLX and SP7, was observed. Additionally, bone marrow-like structures were identified in the central region of the tissue construct, along with CTSK-positive cells and vascular-like structures expressing EMCN (Figure 3G). Overall, our results demonstrate that the skeletal assembloid, which includes IZ/ACP and GPC organoids, can recapitulate the longitudinal bone growth upon transplantation by inducing primary endochondral ossification in the center of assembloids.

DISCUSSION

In this study, we successfully developed a strategy to selectively induce two distinct chondrocyte lineage organoids, namely interzone/articular chondrocyte progenitors (IZ/ACP) and growth plate chondrocytes (GPC) organoids, from hPSCs via ontogenetically defined, expandable limb-bud mesenchymal cells (ExpLBM). Several conventional chondrogenic protocols using BMP2/4 and TGFβ1/3 [18,30,31], including ours [23,24], have been reported previously and yielded mixtures of both articular chondrocyte and growth plate chondrocyte phenotypes (Figure S1B). Here, we discovered that adding the MEK inhibitor PD0325901 with (IZ/ACP condition) preferentially drives cells toward the “interzone/articular cartilage” lineage capable of forming permanent hyaline cartilaginous tissue formation without evidence of ossification, whereas increasing the BMP4 and TGFβ1 concentrations (GPC condition) promotes the “growth plate cartilage” lineage capable of endochondral ossification, giving rise to bone tissue with vasculature and osteoclasts.

MAPK signaling is known to regulate chondrocyte growth, differentiation, and hypertrophy during endochondral ossification [32–34]. Although no evidence has yet demonstrated its importance in generating interzone or articular cartilage progenitors, unbiased chemical screening using GDF5-tdTomato reporter PSCs in this study unveiled this aspect (Figure 1B). In fact, scRNA-seq datasets of the human embryonic limb clearly indicate that MAPK signaling is attenuated during the developmental processes from LBM cells to articular cartilage (Figure S3B). Therefore, in conjunction with scRNA-seq data indicating that our organoids exhibit similar signatures to embryonic limb constituent cells (Figures 1H and 1I), we confirmed that this stepwise induction from PSCs to ExpLBM cells and each differentiated organoid faithfully recapitulate the human developmental program of articular cartilage and growth plate cartilage. Furthermore, in a rat knee defect model, IZ/ACP organoids engrafted into the joint defect area and secreted an extracellular matrix containing ACAN and PRG4, which are characteristic of articular cartilage. Meanwhile, GPC organoids transplanted into a femoral defect model formed cartilage calluses

that underwent endochondral ossification, eventually leading to bone union and partial recovery of mechanical strength. Thus, our protocol not only faithfully recapitulates the in vivo signaling pathways that drive lineage bifurcation during human limb development but also sheds light on providing a promising cell source for regenerative medicine.

An assembloid is an advanced 3D culture model created by combining or fusing multiple organoids. By integrating different types of organoids or cell populations, assembloids aim to recapitulate more complex tissue and organ-like structures and functions than traditional "single-lineage" organoids can offer [35,37]. A further highlight of our study is the generation of a "skeletal assembloid" by fusing IZ/ACP organoids and GPC organoids. When transplanted into immune-deficient mice, the assembloid exhibited longitudinal growth and endochondral ossification at the center, while maintaining cartilage-like tissues at both ends. This arrangement mimics the limb developmental organization, where growth plate cartilage regions are flanked by articular cartilage regions. While several studies have reported the recapitulation of endochondral ossification in cartilage tissue derived from human PSCs [10–14], this is the first demonstration in which the process has been faithfully reproduced in a directional manner along the skeletal longitudinal axis. This model holds great promise for investigating complex human skeletal development as well as for studying pathological conditions affecting both cartilage and bone, such as osteoarthritis and skeletal dysplasia.

Limitation of the study

While this study presents an innovative assembloid approach with human PSCs-derived IZ/ACP and GPC organoids to recapitulate human limb skeletal development, it is important to note certain limitations. Since the longitudinal skeletal growth of the assembloid in this study was observed through subcutaneous transplantation using immune-deficient mice, the functional integration of the transplanted tissue within a normal immune environment and under external factors such as mechanical forces has yet to be elucidated. In fact, we could not observe a secondary ossification center, which typically occurs postnatally in the epiphysis of mammals [36]. Furthermore, given the potential of skeletal assembloid, it is important to utilize this system in future studies to model diseases that cause growth retardation due to impaired limb endochondral ossification.

RESOURCE AVAILABIRITY

Lead contact

Further information and requests for resources and reagents should be directed to and will be fulfilled by the lead contact, Takeshi Takarada (takarada@okayama-u.ac.jp).

Materials availability

tdTomato reporter PSCs derived in this study are available from the lead contact with a completed materials transfer agreement.

Data and code availability

All of the raw sequencing data were deposited in GEO database. These data can be accessed using the GSE accession number GSExxxxx (in progress). This paper also analyzes publicly available data. Accession numbers for these datasets are listed in the STAR Methods section and key resources table. Any additional information and materials will be made available upon request.

ACKNOWLEDGEMENTS

We thank Ayume Nitta, Kokoro Furutani, Aoba Nakajima, Yukio Hitsumoto, Masayuki Okamoto, Yuka Yamamoto and Naoshige Ono for technical assistance; Ziyi Wang and Mitsuaki Ono for their invaluable comments and advice. Preparation of slides and staining was supported by the Central Research Laboratory, Okayama University Medical School. The computation was carried out using the General Projects on supercomputer "Flow" at Information Technology Center, Nagoya University. We thank the members of the Department of Animal Resources, Advanced Science Research Center and Okayama University for maintaining the mice. This research was supported by Grants-in-aid for Scientific Research from the Japan Society for the Promotion of Science (17H04399, 21H02643, 24KK0206 to T. Takarada; 23K08677 to T. Takao), AMED (JP24bm1123059 to T.Takao), JST FOREST Program (JPMJFR225H to T. Takarada), Astellas Foundation for Research on Metabolic Disorders to T.Takao, and the Cooperative Research Program of the Institute for Frontier Life and Medical Sciences, Kyoto University to T. Takarada and J.T. These funders had no role in the study design, data collection and analysis, decision to publish or preparation of the manuscript.

AUTHOR CONTRIBUTIONS

T.Takao and T.Takarada conceived the project and designed experiments. T.O. performed the analysis of sequencing data. K.S. performed organoid transplantation into critical-sized femur defects in SCID rats. D.Y. and Y.F. performed experimetns. M.H. provided critical advice on producing a skeletal assembloid. E.N., T.O. and J.T. discussed the data and provided critical advice. T.Takao and T.Takarada prepared the manuscript.

DECLARATION OF INTERESTS

The authors have filed a patent for the small-molecule combinations reported in this paper.

STAR★METHODS

KEY RESOURCES TABLE

REAGENT or RESOURCE	SOURCE	IDENTIFIER
Antibodies		
Rabbit polyclonal anti-SOX9	Sigma-Aldrich	Cat# AB5535 RRID: AB_2239761
Rabbit polyclonal anti-aggrecan (ACAN)	Proteintech	Cat# 13880-1-AP RRID: AB_2722780
Mouse monoclonal anti-type I collagen (COL1)	SouthernBiotech	Cat# 1441-01 RRID: AB_2794758
Mouse monoclonal anti-type II collagen (COL2)	Thermo Fisher Scientific	Cat# MA1-37493 RRID: AB_2082337
Mouse monoclonal anti-type X collagen (COL10)	Thermo Fisher Scientific	Cat#14-9771-80 RRID: AB_2573017
Rabbit polyclonal anti-PRG4	Novus Biologicals	Cat# NBP1-19048 RRID: AB_2169241
Rabbit monoclonal anti-RUNX2	CST	Cat# 12556 RRID: AB_2732805
Mouse monoclonal anti-SP7	R&D	Cat# MAB7547 RRID: AB_3658831
Rat Anti-Mouse CD107b (LAMP2)	BD Pharmingen	Cat# 550292 RRID: AB_393587
Rabbit monoclonal anti-cathepsin K (CatK)	Abcam	Cat# ab19027 RRID: AB_2261274
Rat monoclonal anti-endomucin (EMCN)	Santa Cruz	Cat# sc-65495 RRID: AB_2100037
Rabbit monoclonal anti-human Vimentin (hVIM)	Abcam	Cat# ab16700 RRID: AB_443435
Mouse monoclonal anti-human Nucleoli (hNuc)	Abcam	Cat# ab190710 RRID: AB_2937055
Rabbit polyclonal anti- Kusabira-Orange 2 (KuO)	MBL	Cat# PM051M RRID: AB_2876863
Rabbit polyclonal anti-Histone H3K27ac	Active Motif	Cat# 39134 RRID: AB_2722569
Rabbit polyclonal anti-Histone H3K27me3	Active Motif	Cat# 39155 RRID: AB_2561020
Goat Anti-mouse IgG (H+L), F(ab')2 Fragment (Alexa Fluor 647 Conjugate)	CST	Cat# 4410S
Goat Anti-rabbit IgG (H+L), F(ab')2 Fragment (Alexa Fluor 488 Conjugate)	CST	Cat# 4412S
Goat Anti-rabbit IgG (H+L), F(ab')2 Fragment (Alexa Fluor 647 Conjugate)	CST	Cat# 4414S
Goat Anti-rat IgG (H+L), (Alexa Fluor 488 Conjugate)	CST	Cat# 4416S
Goat Anti-rat IgG (H+L), (Alexa Fluor® 647 Conjugate)	CST	Cat# 4418S
Chemicals, peptides, and recombinant proteins		
CHIR99021	AxonMedchem	Cat# Axon1386
PIK-90	Selleck	Cat# S1187
A 83-01	Tocris	Cat# 2939
Wnt-C59	Cellagen Technology	Cat# C7641-2s
LDN-193189	ReproCELL	Cat# 04-0074
GDC-0449 (Vismodegib)	Cellagen Technology	Cat# C4044-5
Y-27632	MedchemExpress	Cat# MCE HY-10583
SAG 21k	R&D	Cat# 5282
ATRA	Sigma-Aldrich	Cat# R2625
XAV-939	Selleck	Cat# S1180
SF1670	Cayman	Cat# 15368
MK-2206	Cayman	Cat# 11593
PD0325901	Selleck	Cat# S1036

VO-OHpic	Cayman	Cat# 10009965
MHY1485	Cayman	Cat# 18008
DAPT	Wako	Cat# 043-33581
Rapamycin	Selleck	Cat# S1039
Recombinant human Activin A	R&D	Cat# 338-AC
Recombinant human BMP4	R&D	Cat# 314-BP
Recombinant human TGFβ1	PEPROTECH	Cat# 100-21C
Recombinant human GDF5	PEPROTECH	Cat# 120-01
Recombinant human FGF2	Katayama Chemical	Cat# 161-0010
Recombinant human EGF	STEMCELL TECHNOLOGIES	Cat# ST-78006
Critical commercial assays		
RNeasy Mini Kit	QIAGEN	Cat# 74106
ReverTra Ace qPCR RT Master Mix with gDNA Remover	TOYOBO	Cat# FSQ-301
Luna Universal qPCR Master Mix	NEB	Cat# M3003X
KAPA RNA HyperPrep kit with RiboErase (HMR)	Nippon Genetics	Cat# KK8561
SeqCap Adapter Kit (Set A/B)	Roche	Cat# 07141530001 Cat# 07141548001
Chromium Next GEM Single Cell 3′ GEM kit v.3.1	10x Genomics	Cat# 1000269
Chromium Next GEM Single cell G tip kit	v	Cat# 1000127
Dual index kit TT set A	10x Genomics	Cat# 1000215
High sensitivity D5000 screen tape	Agilent	Cat# 5067-5592
Illumina Tagment DNA Enzyme and Buffer	Illumina	Cat# 20034197
MinElute PCR purification kit	QIAGEN	
Nextera Index Kit	Illumina	Cat# 15055290
CUT&TAG-IT Assay Kit, Anti-Rabbit	Active Motif	Cat# 53160
RNAscope Multiplex Fluorescent Reagent Kit ver. 2	Advanced Cell Diagnostics	Cat# 323100
GFP probe (RNAscope)	Advanced Cell Diagnostics	Cat# 538851
TSA Vivid Fluorophore 570 (RNAscope)	Advanced Cell Diagnostics	Cat# 323272
Deposited data		
Raw and analyzed data (BulkRNA-seq, scRNA-seq, ATAC-seq, and CUT&Tag)	This study	GSExxxxx (in progress)
Human limb-bud data (scRNA-seq)	Zhang et al. [27]	E-MTAB-8813
Stepwise differentiation data from hiPSC into cartilage (BulkRNA-seq)	Yamada et al. [23]	GSE165620
Experimental models: Cell lines		
414C2 hiPSCs	CiRA, Kyoto University	N/A
SEES4 hESCs	RIKEN BRC	HES0017
802-3G hiPSCs	Reprocell	RCRP004N
GDF5$^{3'tdTomato}$ -reporter 414C2 hiPSCs	This paper	N/A
SP7$^{3'tdTomato}$ -reporter SEES4 hESCs	This paper	N/A
CAG-GFP hiPSCs	This paper	N/A
CAG-KuO hiPSCs	This paper	N/A
Experimental models: Organisms/strains		
NOD SCID mouse (NOD.Cg-*Prkdc*^{scid}/J)	The Jackson Laboratory, Japan	N/A
C57BL/6J mouse	CLEA Japan	N/A
SCID rat (F344-*Il2rg*^{em1Iexas})	Laboratory Animal Research, The University of Tokyo	Cat# 12076-002
Oligonucleotides		
Primers for RT-qPCR and genotyping, see Table S1.	This paper	N/A

Recombinant DNA		
pPB-CAG-DEST-pA-pgk-bsd	Addgene	#74918
KW158 (PCAG-PBase)	Kim et al. [38]	Kindly provided by Dr. Knut Woltjen
pSpCas9(BB)-2A-Puro (PX459) V2.0	Addgene	#62988
PX459-GDF5 gRNA	This paper	N/A
PX459-SP7 gRNA	This paper	N/A
pUCFa-GDF5 3′HA HA-IRES-tdTomato-PGK-Neo	This paper	N/A
pTA2-SP7 3′HA HA-IRES-tdTomato-PGK-Neo	This paper	N/A
Software and algorithms		
GraphPad Prism 8	GraphPad software	https://www.graphpad.com/
Fastp (version 0.23.4)	OpenGene	https://github.com/OpenGene/fastp
Kallisto (version 0.48.0)	Pachter Lab	https://pachterlab.github.io/kallisto/
Bowtie2 (version 2.2.5)	Quinlan lab	https://bowtie-bio.sourceforge.net/bowtie2/index.shtml
Gopeaks (version 1.0.0)	Maxson Braun Lab	https://github.com/maxsonBraunLab/gopeaks
Bedtools (version 2.30.0)	Quinlan Lab	https://github.com/arq5x/bedtools2
Homer (version 4.11)	Benner Lab	http://homer.ucsd.edu/homer/
deeptools (version 3.5.1)	Max Planck Institute	https://github.com/deeptools/deepTools
Cell Ranger (version 7.0.1)	10x Genomics	https://www.10xgenomics.com/jp/support/software/cell-ranger/latest
R (version 4.1.3)	R Foundation	https://www.r-project.org/
edgeR (version 4.0.3)	Smyth Lab	https://github.com/OliverVoogd/edgeR
NOISeq (version 2.46.0)	Conesa Lab	https://github.com/ConesaLab/NOISeq
Seurat (version 5.0.3)	Satija lab	https://satijalab.org/seurat/
DoubletFinder (version 2.0.4)	Git Hub	https://github.com/chris-mcginnis-ucsf/DoubletFinder
Other		
StemFit	Ajinomoto	Cat# AK02N
DMEM	Wako	Cat# 048-29763
IMDM, GlutaMAX_ supplement	Thermo Fisher Scientific	Cat# 31980097
Ham's F-12 Nutrient Mix, GlutaMAX_ supplement	Thermo Fisher Scientific	Cat# 1765092
Polyvinyl alcohol	Sigma-Aldrich	Cat# P8136-250G
Chemically defined lipid concentrate (CD lipid concentrate)	Thermo Fisher Scientific	Cat# 11905031
Monothioglycerol	Sigma-Aldrich	Cat# M6145
Insulin	Sigma-Aldrich	Cat# 11376497001
Transferrin	Roche	Cat# 10652202001
L(+)-Ascorbic acid	Wako	Cat# 014-04801
Insulin-transferrin-selenium (ITS) 100x	Thermo Fisher Scientific	Cat# 41400045
Fetal bovine serum (FBS)	Gibco	Cat# 10270106 (Lot:42F5094K)
iMatrix-511 silk (iMatrix)	MATRIXOME	Cat# 892021
Human plasma fibronectin (1 mg/ml)	Sigma-Aldrich	Cat# FC010
Penicillin-streptomycin (10,000 U/mL)	Thermo Fisher Scientific	Cat# 15140122
G418	Life Technologies	Cat# 076-05962
TrypLE Select	Thermo Fisher Scientific	Cat# 12563029
Accutase	NACALAI TESQUE	Cat# 12679-54
Collagenase, Type II, powder	Gibco	Cat# 17101015
0.5 M EDTA (pH8.0) solution	NIPPON GENE	Cat# 311-90075
96-well clear ultra-low attachment microplates	CORNING	Cat# 7007
Agarose, Low Gelling Temperature	Sigma-Aldrich	Cat# A9414-5G

4',6-diamidino-2-phenylindole (DAPI)	Thermo Fisher Scientific	Cat# D3571
Calcein-AM	DOJINDO	Cat# C326
In-Fusion HD Cloning Kit	Takara	Cat# Z9648N
KOD FX NEO Kit	Takara	Cat# KFX-201
pTA2 vector (TArget Clone™)	TOYOBO	Cat# TAK-101
4% paraformaldehyde (PFA)	Wako	Cat# 163-20145
Hematoxylin	Wako	Cat# 131-09665
Eosin	Wako	Cat# 051-06515
Safranin O	Wako	Cat# 530-00592
Fast green	Wako	Cat# 061-00031
Silver nitrate	Wako	Cat# 195-09382
Entellan™ new	Merck	Cat# 1079610100
Normal goat serum (NGS)	Vector laboratories	Cat# S-1000-20
Fluoromount-G	SouthernBiottech	Cat# 0100-01

EXPERIMENTAL MODEL AND STUDY PARTICIPANT DETAILS

Animals

The experiments involving mice and rats were approved by the Okayama University Animal Care and Use Committee. Immunodeficient NOD-SCID mice and SCID rats were purchased from The Jackson Laboratory (Japan) and Laboratory Animal Research (The University of Tokyo), respectively. The animals were housed under a 12-hour light/12-hour dark cycle (06:00–18:00) in a temperature-controlled room maintained at 22 ± 1°C with 40–60% humidity. Food and water were provided ad libitum."

Cell lines

hPSC lines and maintenance

The hPSCs were cultured or maintained with StemFit (Ajinomoto). Before reaching subconfluency, cells were dissociated with TrypLE Select (Thermo Fisher Scientific)/0.25 mM EDTA and suspended in StemFit containing 10 μM Y-27632 (MedchemExpress) . Cells (1 ×10^4) were suspended in StemFit containing 10 μM Y-27632 and 8 μl iMatrix (human laminin-511 E8 fragment, MATRIXOME) and added to a 6-cm dish. Culture media were the next day with fresh StemFit without Y27632. Culture media were changed every 2 days until the next passage. The following hPSC lines were used: 414C2 hiPSCs were provided by the Center for iPS Cell Research and Application, Kyoto University, Japan; 802-3G hiPSCs were purchased from Riprocell (Japan). SEES4 hESCs were donated by RIKEN BRC (Japan).

Generation of a GDF5$^{3'tdTomato}$ and SP7$^{3'tdTomato}$ -reporter cell line

The targeting strategy for knock-in of the IRES-tdTomato-PGK-Neo cassette at the *GDF5* 3′-UTR or *SP7* 3′-UTR or to achieve bicistronic expression of GDF5/SP7 and tdTomato is shown in Figure

S2A. The *GDF5* 3′ homology region (GDF5 3′HA) was obtained by artificial gene synthesis service (pUCFa-GDF5 3′HA vector) (FASMAC). To construct the targeting vector (pUCFa-GDF5 3′HA HA-IRES-tdTomato-PGK-Neo), IRES-tdTomato-PGKNeo fragments were inserted into pUCFa-GDF5 3′HA vector using an In-Fusion HD Cloning Kit (Takara). Guide RNAs (gRNAs) were designed to target the PAM sequence located 161 bp downstream from the stop codon of GDF5 (CTGAGTGTGACTTGGGCTAAAGG, underline indicates the PAM sequence). gRNA oligos (Table S1) were designed, phosphorylated, annealed and subcloned into the PX459 vector (Addgene) harboring a Cas9 expression cassette (PX459-GDF5 gRNA). The *SP7* 3′ homology region (SP7 3′HA) was synthesised using PCR with a KOD FX NEO Kit (Takara). Genomic DNA extracted from 414C2 hiPSCs, which served as a template, was ligated with pTA2 vector (TOYOBO) using TA cloning (pTA2-SP7 3′HA vector). To construct the targeting vector (pTA2-SP7 3′HA HA-IRES-tdTomato-PGK-Neo), IRES-tdTomato-PGKNeo fragments were inserted into pTA2-SP7 3′HA vector using an In-Fusion HD Cloning Kit (Takara). Guide RNAs (gRNAs) were designed to target the PAM sequence located 104 bp downstream from the stop codon of *SP7* (CCCATGCATGCCATCCTTCGGGG, underline indicates the PAM sequence). gRNA oligos (Table S1) were designed, phosphorylated, annealed and subcloned into the PX459 vector (Addgene) harboring a Cas9 expression cassette (PX459-SP7 gRNA).

To generate the GDF5$^{3'tdTomato}$ or SP7$^{3'tdTomato}$ -reporter line, 1 × 10^6 414C2 hiPSCs (GDF5$^{3'tdTomato}$-reporter) or SEES4 hESCs (SP7$^{3'tdTomato}$-reporter) were electroporated with targeting vector (7.5 μg) and Cas9/gRNA expression vector (2.5 μg). Selection with G418 (Life Technologies) was maintained for 10 days until stable colonies appeared. Colonies with diameters of >500 μm were selected using a P10 pipette tip with the aid of a microscope and used to inoculate larger volumes of media. To verify precise integration of IRES-tdTomato-PGKNeo cassette into the GDF5/SP7 3′UTR locus, the 5′ or 3′ ends between GDF5/SP7 and IRES-tdTomato-PGKNeo cassette were amplified for nucleotide sequence analysis. The PCR primers used are listed in Table S1.

Generation of CAG-GFP and CAG-KuO-reporter cell line

For the generation of CAG-GFP hiPSC and CAG-KuO hiPSC reporter lines, 1×10^6 single cells dissociated from 414C2 hiPSCs were electroporated with 5 μg of piggyBac Transposase expression plasmid (PCAG-PBase, kindly provided by Dr. Knut Woltjen) [38] and 5 μg of donor plasmids (either pPB-CAG-GFP or pPB-CAG-KuO plasmid) using the Super Electroporator NEPA21 Type II (NEPAGENE), and then plated onto iMatrix-coated plate. Three days after electroporation, cells were treated with puromycin for 1 week and allowed for recovery for another 5~7 days. Then, GFP^+ or KuO^+ clones were picked and expanded.

METHOD DETAILS

Generation of ExpLBM cells from hPSCs.

For step-wise differentiation into LBM cells [23,24], hPSCs (3×10^4) were suspended in 1 ml of StemFit (Ajinomoto) containing 10 μM Y-27632 (MedchemExpress), and 4 μl of iMatrix was added to a 3.5-cm culture dish. The culture medium was replaced the next day with fresh StemFit without Y27632. After culturing for 2 days, the cells were washed with PBS, and differentiation was induced by changing the following culture medium based with chemically defined CDM2 medium at each time point as described previously [24]. In brief, cells were treated with mid-primitive streak (MPS) medium (CDM2 basal medium + 30 ng/ml ACTIVIN A + 40 ng/ml BMP4 + 6 μM CHIR99021 + 100 nM PIK-90 + 10 μM Y27632) for 1 day to induce MPS cells (day 1), LPM medium (CDM2 medium + 1 μM A 83-01 + 30 ng/ml BMP4 + 1 μM C59 + 10 μM Y-27632) for 1 day to induce LPM cells (day 2), and finally LBM medium (CDM2 basal medium +1 μM A 83-01 + 0.5 μM LDN-193189 + 3 μM CHIR99021 + 150 nM Vismodegib + 10 μM Y-27632) for 2 days to induce LBM cells (day 4). The composition of CDM2 basal medium was as follows: 50% IMDM (+ GlutaMAX + HEPES + sodium bicarbonate; Gibco) + 50% F12 (+GlutaMAX) + 1 mg/ml polyvinyl alcohol (Sigma-Aldrich) + 1% CD lipid concentrate (Gibco) + 450 μM monothioglycerol (Sigma-Aldrich) + 7 μg/ml insulin (Sigma-Aldrich) + 15 μg/ml transferrin (Roche) + 1% v/v penicillin/streptomycin (Thermo Fisher Scientific). For generation of ExpLBM cells, LBM cells were dissociated using accutase (NACALAI TESQUE), and 2×10^5 cells were suspended in ExpLBM medium (CDM2 basal medium + 3 μM CHIR99021 + 1 μM A 83-01 + 20 ng/ml FGF2 (Katayama Chemicals) + 20 ng/ml EGF (STEMCELL TECHNOLOGIES) + 10 μM Y-27632) and cultured on a 6-cm dish coated with 4 μg/mL of human plasma fibronectin (Sigma-Aldrich). The culture media was replaced with a fresh ExpLBM medium every 2 days. Before reaching subconfluence, the cells were passaged as described above. The details of the human recombinant proteins and small molecule agonists or inhibitors are listed in key resources table.

Chondrogenic Induction (generation of IZ/ACP organoid, GPC organoid and skeletal assembloid)

To perform chondrogenic induction of ExpLBM cells under pellet culture conditions (3DCI), 2×10^5 ExpLBM cells were suspended in 200 μL of Step1 medium [CDM2 medium + 3 μM CHIR99021 + 10 ng/mL FGF2 + 50 μg/mL ascorbic acid (Wako) + 1× insulin-transferrin-selenium (ITS) (Thermo Fisher Scientific)] and plated into 96-well ultra-low U-bottom plates (CORNING). The cells were pelleted by centrifugation at 2,000 rpm for 5 minutes. Six days after culture, the culture medium was changed to Step 2 medium [CDM2 medium + 50 μg/mL ascorbic acid + 1× ITS + 30 ng/mL BMP4 (R&D) + 10 ng/mL TGFβ1 (PEPROTECH) + 10 ng/mL GDF5

(PEPROTECH) + 10 ng/mL FGF2] and cultured for an additional 6 days. Subsequently, the medium was replaced with Step 3 medium [CDM2 medium + 50 μg/mL ascorbic acid + 1× ITS + 30 ng/mL BMP4 + 10 ng/mL TGFβ1 + 10 ng/mL GDF5] and maintained for 14 days in the presence of various tested chemicals. To generate IZ/ACP organoid, we used Step 3 medium supplemented with 500 nM PD0325901 (#16 condition, Figure 1B). GPC organoids were generated using the following medium [CDM2 medium + 50 μg/mL ascorbic acid + 1× ITS + 300 ng/mL BMP4 + 100 ng/mL TGFβ1 + 10 ng/mL GDF5] during the 14-day Step 3 period (#2 condition, Figure 1B). The culture medium was refreshed with fresh medium every 3 days. To generate the skeletal assembloid, two IZ/ACP organoids were positioned vertically at both ends of a GPC organoid within low-melting point agarose gel (Sigma) and then cultured in DMEM (Wako) supplemented with 10% FBS and 1% v/v penicillin/streptomycin (Thermo Fisher Scientific) for 7 days to allow spontaneous fusion of these samples, referred to as skeletal assembloid. The media were changed every other day.

Bulk RNA-seq and data processing

Total RNA was extracted using a RNeasy mini kit (QIAGEN), and sequencing libraries were prepared using a KAPA RNA HyperPrep Kit with RiboErase (HMR) (Nippon Genetics) and a SeqCap Adapter Kit (Set A or Set B) (Roche) following the manufacturer's instructions. Sequencing was performed using NovaSeq 6000 (Illumina) with a pair-read sequencing length of 150 bp. All sequence reads were extracted in FASTQ format using the CASAVA 1.8.4 pipeline. Fastp (v0.23.4) was used to remove adapters and filter raw reads of < 60 bases in addition to leading and trailing bases with a read quality of less than 30. For the pseudoalignment of the filtered reads to the GRCh38, Kallisto (v0.48.0) was used. GeTMM normalization was performed using edgeR (v4.0.3) to account for sample variation. Differentially expressed genes were identified through NOISeq (v2.46.0) analysis with a threshold of prob > 0.8 and abs(Log2FC) > 1. For hiPSC to ExpLBM, our previous data were reanalyzed (GSE165620).

ATAC-seq and data processing

ATAC-seq was conducted following the method previously described [39]. In brief, 4,000 cells were collected and lysed using lysis buffer containing 10 mM Tris-HCl, 10 mM NaCl, 3 mM MgCl2, and 0.1% IGEPAL CA-630. Tn5 transposase reaction using the Illumina Tagment DNA Enzyme and Buffer (Illumina) was carried out at 37C for 30 min. The reacted DNA was purified using a MinElute PCR purification kit (QIAGEN) and amplified for 8–15 cycles using Nextera Index Kit (Illumina) to produce libraries for sequencing. Sequencing was performed using HiSeq1500 (Illumina) with a pair-read sequencing length of 150 bp. Two or three biological replicates were analyzed. Sequences were aligned to human genome sequences (hg38) using Bowtie2 with default

parameters. Gopeaks was used to call peaks using default parameters. Regions where overlapping peaks were identified by Bedtools intersect between biological replicates were designated as high-confidence peaks. Read count matrix of each sample was used for detection of differentially accessible peaks by using edgeR. For the heatmap, normalized read counts obtained using edgeR were z-score-scaled and plotted. For motif analysis, findMotifsGenome.pl of Homer was used with the -size200-mask option. For the annotation of peaks, annotatePeaks.pl of Homer was used with the default settings. For visualization, BAM files are converted to bigwig format using deeptools with the command “bamCoverage -binSize 1 -normalizeUsing RPGC --extendReads”.

CUT&Tag of histone modification, and data processing

A total of 20,000 cells were collected as input, and libraries were prepared using CUT&Tag-IT Assay Kit (Active Motif) following to manufacturer’s protocol. Anti-H3K27ac (Active Motif) and anti-H3K27me3 (Active Motif) were used for reactions. Three biological replicates were analyzed. Sequencing was performed using HiSeq1500 (Illumina) with a pair-read sequencing length of 150 bp. Sequences were aligned to human genome sequences (hg38) using Bowtie2 (parameters: --end-to-end, --very-sensitive, --no-mixed, --no-discordant, --phred33, -I 10, -X 700). For the peak calling, gopeaks and bedtools intersect were utilized in the same way as described in the section on ATAC-seq. BAM files are converted to bigwig format using deeptools with the command “bamCoverage -binSize 1 -normalizeUsing RPGC --extendReads”. Heatmap was created using deeptools “computeMatrix” and “plotHeatmap” functions. To separate the promoter and non-promoter regions, we used the “annotatePeaks.pl” function of the Homer program and defined a promoter as one that was annotated as a promoter-TSS in the default setting.

***in vivo* transplantation**

For subcutaneous transplantation, organoids and assembloids were transplanted into immunodeficient NOD-SCID mice. For transplantation into osteochondral defects created in the knee joint articular cartilage, the joint capsules of the knee joint of 10- week-old SCID rats (F344-Il2rgem1Iexas) were opened. A drill hole with a 1-mm diameter and a 0.5-mm depth was created at the femoral groove. Organoids were transplanted into the osteochondral defect of the articular cartilage via press fitting. The joint capsules were closed, and the rats were sacrificed 3 months thereafter. For transplantation into critical-sized femur defects in SCID rats, a critical-size defect measuring 5 mm was created in the midshaft of the femur using a drill. The created defect was stabilized using an external fixator, and the large GPC organoids were implanted into the defect. For postoperative evaluation of bone regeneration, radiographic imaging and histological analysis were performed 1 and 3 months after surgery.

The transplanted tissues were harvested and fixed with 4% PFA (Wako) for 24 h. Tissue samples were paraffin-embedded at the Central Research Laboratory, Okayama University Medical School. For hematoxylin and eosin staining, deparaffinized sections were stained with hematoxylin (Wako) for 20 min and eosin (Wako) for 1 min. For Safranin O staining, the deparaffinized sections were stained with 0.05% fast green (Wako) solution for 5 min and then with 0.1% Safranin O (Wako) solution for 5 min. For von kossa staining, fixed samples were incubated in 5% silver nitrate (Wako) under sunlight for 60 minutes, followed by treatment with 5% sodium thiosulfate for 3 minutes. After staining, the samples were dehydrated and embedded with Entellan new reagent (Merck). Images were acquired using a BZ-X710 microscope (Keyence).

Flow cytometry

Following dissociation with Accutase, 1×10^5 cells were suspended in 100 μl of 2% FBS/PBS and incubated with antibody (diluted 200×) for 1 h on ice. Fluorescence was detected using a CytoFLEX S flow cytometer (Beckman Coulter), and data were analyzed using FlowJo software (FlowJo LLC). The antibodies used are listed in key resources table.

Real-time quantitative RT-PCR (RT-qPCR)

Total RNA was extracted using a RNeasy mini kit, and cDNA was synthesized using ReverTra Ace qPCR RT Master Mix with gDNA Remover (TOYOBO) according to manufacturer's protocol. cDNAs were then used as templates for qPCR analysis with Luna Universal qPCR Master Mix (NEB) and gene-specific primers. qPCR was performed using an AriaMX Real-Time PCR System (Agilent). The cycle parameters were as follows: denaturation at 95 °C for 30 seconds, annealing at 62 °C for 30 seconds and elongation at 72 °C for 30 seconds. The expression level of each gene was calculated using the $2^{-\Delta\Delta Ct}$ method. The primer sequences are described in Table S1.

Immunohistochemistry

Tissues were fixed with a 4% PFA, and paraffin-embedded samples were sectioned (4 μm thick). Tissue samples were deparaffinized, and antigens were activated by heating slides in 10 mM citrate buffer (pH 6.0). Samples were incubated with blocking solution [3% NGS (Vector laboratories)/0.1% Triton X-100/1× PBS (−)]. Samples were treated with primary antibody (diluted 1:200) overnight at 4°C and were incubated with a blocking solution [(3% NGS)/0.1% Triton X-100/1× PBS (−)], followed by secondary antibody (diluted 1:400) for 1 hour at room temperature. Samples were embedded with Fluoromount-G (SouthernBiottech) after staining with DAPI (Thermo Fisher Scientific) and the images were acquired using the BZ-X710 camera. The antibodies are listed in key resources table.

scRNA-seq and data processing

ExpLBM cells were washed with PBS (−) and dissociated with Accutase at 37 °C for 5 min, while IZ/ACP and GPC organoids were washed with PBS (−) and then treated with 900 unit/ml collagenase (type II) (Gibco) for 60 minutes at 37 °C, followed by gentle pipetting using a serological pipette to dislodge and dissociate aggregates. Cell sorting was performed on a FACSAria III Cell Sorter (BD Biosciences) to remove dead cells and debris via forward scatter, side scatter, and DAPI/Calcein-AM staining. The number of the cells forwarded to the analysis was 10,000 cells. A Chromium Next GEM Single Cell 3′ GEM Kit v3.1 (10x Genomics) was used for library preparation. Dissociated cells were separated into single droplets with unique molecular barcodes and then processed following the manufacturer's protocol. Quality checks of the samples were performed using the High sensitivity D5000 screen tape (Agilent) and Agilent 4150 TapeStation system (Agilent). Sequencing was performed using a DNBseq (MGI).

To obtain count matrices, reads were aligned to the human genome GRCh38 using Cell Ranger (v7.0.1) with the default parameters. Downstream analysis was performed using the R package Seurat (v5.0.3) [40]. For quality control, cells with detected genes over 5, UMI count over 5, and the fraction of mitochondrial genes <10% were kept as high-quality cells. Doublets were detected using DoubletFinder (v2.0.4) [41] and removed. Counts were normalized, and then the top 3000 highly variable genes were detected (SCTransform and FindVariableFeatures function in Seurat).

For data integration, the batch effect was removed by LeverageScore method by SketchData in the Seurat. After scaling gene expression and performing dimensional reduction, we visualized cells using Uniform Manifold Approximation and Projection (UMAP) embedding. Cluster annotations were labeled with canonical markers.

We compared the transcriptome similarity with published developing human limb (5–9 postconceptional weeks (pcw)) scRNA-seq data using anchor-based label transfer implemented in Seurat. To do that, anchors between the query and reference dataset were identified and filtered using the FindTransferAnchors function with the top 14 dimensions. Then, the prediction score was calculated using the TransferData function. The cell type and region similarity (defined as the mean prediction score of each cell type) were visualized with a heatmap.

We performed trajectory analysis using the monocle3 package (v1.3.7) [42] with default parameters, and the Mes1 cluster was chosen as the root node to order cells. The pseudotime heatmap was plotted using the ComplexHeatmap (v2.18.0) package.

Scanning Electron Microscopy (SEM) and Transmission Electron Microscopy (TEM)

For SEM, samples were fixed overnight in 2% PFA and 2% glutaraldehyde in 0.1 M phosphate

buffer (pH 7.4) at 4 °C. After washing, samples were post-fixed with 2% osmium tetroxide for 90 minutes at room temperature. Following washing, the tissues were dehydrated using a series of ascending ethanol solutions (30%, 50%, 70%, 90%, and two changes of 100%) for 10, 10, 10, 30, 30, and 30 minutes, respectively. Dehydrated tissues were immersed in t-butyl alcohol for 30 minutes and freeze-dried using an EIKO ID-2 freeze dryer. The dried samples were cracked with a razor blade to expose the photoreceptor layer and mounted on the aluminum sample stage. The sample surfaces were coated with osmium using HPC-1SW (vacuum device). Subsequently, the samples were analyzed using a Hitachi S-4800 scanning electron microscope. For TEM, cartilaginous particles were fixed with 4% PFA and 2% glutaraldehyde, followed by postfixation with 2% osmium tetroxide. After dehydration, embedding, and polymerization, ultra-thin sections were stained with 2% uranyl acetate and observed using a Hitachi H-7100S transmission electron microscope at an acceleration voltage of 80 kV.

in situ hybridization (ISH)

The paraffin sections were stained for GFP using an RNAscope Multiplex Fluorescent Reagent Kit ver. 2 (Advanced Cell Diagnostics). More precisely, the sections were pretreated with RNAScope hydrogen peroxidase for 10 min at room temperature, with RNAScope Target Retrieval for 15 min at 98 °C, and with protease plus treatment for 30 min at 40 °C. The sections were then hybridized with GFP probe (Advanced Cell Diagnostics) for 2 h at 40 °C, and amplified through 6 sequential steps according to the instructions provided by the manufacturer. The probe signal was visualized with TSA Vivid Fluorophore 570 (Advanced Cell Diagnostics). Then, the slides were observed using the BZ-X710 camera.

μCT analysis

For the analysis of critical-sized femoral defects in SCID rats, the imaging was performed by a maicro-CT system, Latheta LCT-200 (Hitachi Aloka Medical) with voltage of 50 kV, current of 200 μA. For the analysis of skeletal assembloids, the scans were performed on the ScanXmate-L090HH (Comscan tecno) with voltage of 74 kV, current of 100 μA. The resolution was 11.906 μm per pixel. Three-dimensional images were reconstructed using VXRE, VX3D (3D Industrial Imaging) and TRI/3D-BON-FCS (RATOC System Engineering).

QUANTIFICATION AND STATISTICAL ANALYSIS

Data were analyzed using Prism 8. All data were acquired by performing biological replicates of two or three independent experiments and are presented as the mean ± standard error of the mean. Statistical significance was determined using an ordinary one-way analysis of variance with correction for multiple testing using the Turkey method.

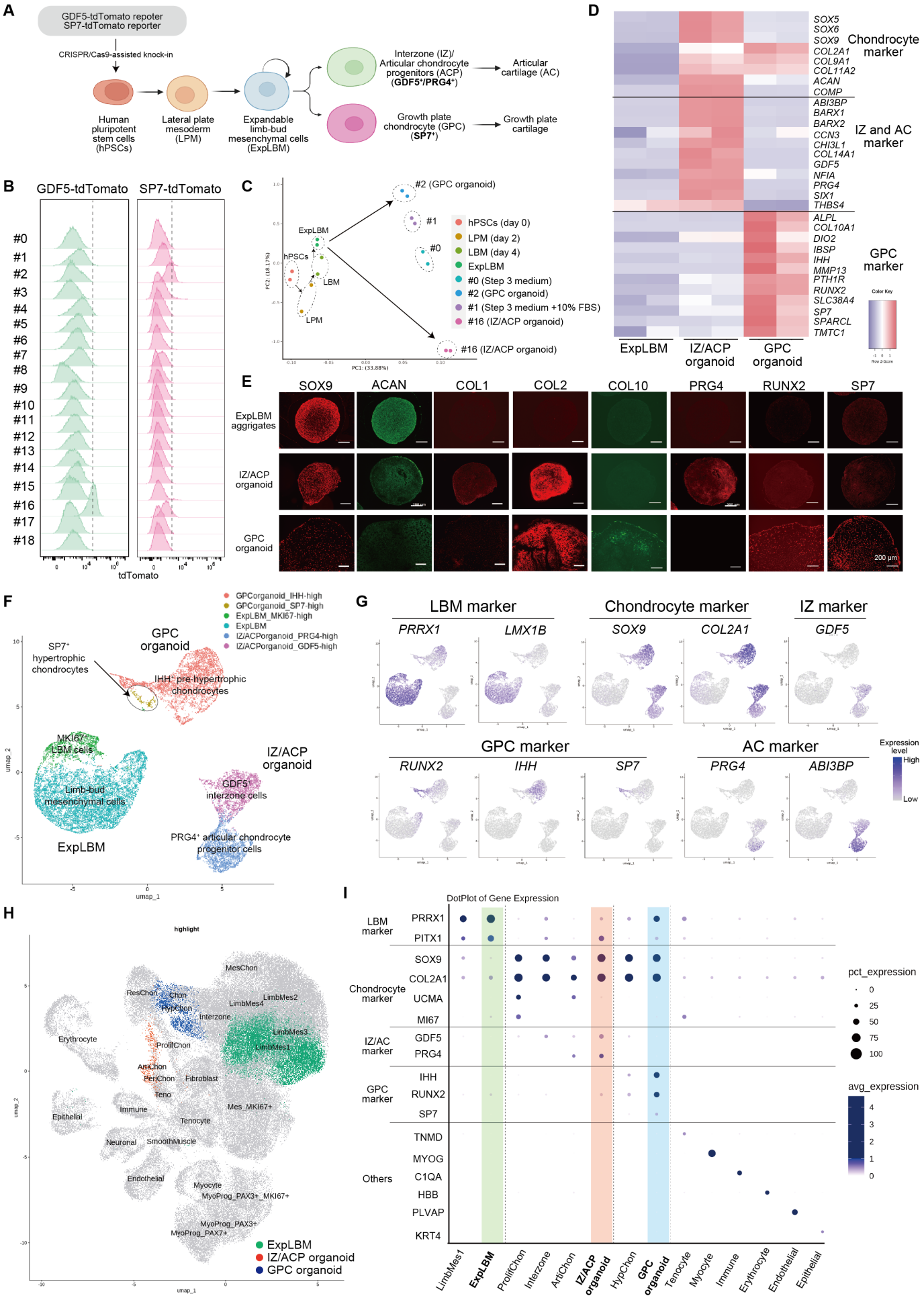
A
GDF5-tdTomato repoter
SP7-tdTomato reporter
CRISPR/Cas9-assisted knock-in
Human pluripotent stem cells (hPSCs)
Lateral plate mesoderm (LPM)
Expandable limb-bud mesenchymal cells (ExpLBM)
Interzone (IZ)/ Articular chondrocyte progenitors (ACP) (GDF5+/PRG4+)
Articular cartilage (AC)
Growth plate chondrocyte (GPC) (SP7+)
Growth plate cartilage
B
GDF5-tdTomato
SP7-tdTomato
tdTomato
C
#2 (GPC organoid)
#1
#0
ExpLBM
hPSCs
LBM
LPM
#16 (IZ/ACP organoid)
hPSCs (day 0)
LPM (day 2)
LBM (day 4)
ExpLBM
#0 (Step 3 medium)
#2 (GPC organoid)
#1 (Step 3 medium +10% FBS)
#16 (IZ/ACP organoid)
PC1: (33.88%)
PC2: (18.17%)
D
Chondrocyte marker
IZ and AC marker
GPC marker
ExpLBM
IZ/ACP organoid
GPC organoid
E
SOX9
ACAN
COL1
COL2
COL10
PRG4
RUNX2
SP7
ExpLBM aggregates
IZ/ACP organoid
GPC organoid
200 μm
F
GPCorganoid_IHH-high
GPCorganoid_SP7-high
ExpLBM_MKI67-high
ExpLBM
IZ/ACPorganoid_PRG4-high
IZ/ACPorganoid_GDF5-high
GPC organoid
SP7+ hypertrophic chondrocytes
IHH+ pre-hypertrophic chondrocytes
MKI67+ LBM cells
Limb-bud mesenchymal cells
ExpLBM
IZ/ACP organoid
GDF5+ interzone cells
PRG4+ articular chondrocyte progenitor cells
umap_1
umap_2
G
LBM marker
PRRX1
LMX1B
Chondrocyte marker
SOX9
COL2A1
IZ marker
GDF5
GPC marker
RUNX2
IHH
SP7
AC marker
PRG4
ABI3BP
Expression level
High
Low
H
highlight
MesChon
ResChon
Chon
HypChon
LimbMes4
LimbMes2
Interzone
LimbMes3
LimbMes1
Erythrocyte
ProlifChon
ArtiChon
PeriChon
Fibroblast
Teno
Immune
Mes_MKI67+
Epithelial
Tenocyte
Neuronal
SmoothMuscle
Endothelial
Myocyte
MyoProg_PAX3+_MKI67+
MyoProg_PAX3+
MyoProg_PAX7+
ExpLBM
IZ/ACP organoid
GPC organoid
umap_1
umap_2
I
DotPlot of Gene Expression
LBM marker
PRRX1
PITX1
Chondrocyte marker
SOX9
COL2A1
UCMA
MI67
IZ/AC marker
GDF5
PRG4
GPC marker
IHH
RUNX2
SP7
Others
TNMD
MYOG
C1QA
HBB
PLVAP
KRT4
LimbMes1
ExpLBM
ProlifChon
Interzone
ArtiChon
IZ/ACP organoid
HypChon
GPC organoid
Tenocyte
Myocyte
Immune
Erythrocyte
Endothelial
Epithelial
pct_expression
0
25
50
75
100
avg_expression
4
3
2
1
0

Figure 1

Figure 1: *in vitro* stepwise induction of hPSC-derived limb-bud mesenchymal (LBM) cells into interzone/articular chondrocyte progenitors (IZ/ACP) and growth plate chondrocyte (GPC) organoid.

(A) Overview of the stepwise induction and differentiation of human LBM cells, followed by the subsequent chondrocyte lineages, closely mimicking embryonic development. We determined the optimal conditions for ExpLBM cells to induce IZ/ACP and GPC organodis using GDF5- or SP7-tdTomato reporters, respectively.

(B) tdTomato fluorescent intensity in GDF5$^{3'tdTomato}$ or SP7$^{3'tdTomato}$ -reporter-derived ExpLBM cells treated with 18 combinations of chemicals and cytokines for 14 days in the presence of 30 ng/mL BMP4 and 10 ng/mL TGFβ1. #0, none; #1, 10%FBS; #2, 300 ng/mL BMP4+100 ng/mL TGFβ1+10%FBS; #3, CHIR99021 (GSK3b inhibitor, WNT activator); #4, C59 (PORCN inhibitor, WNT inhibitor); #5, XAV-939 (tankyrase 1 inhibitor, WNT inhibitor); #6, LDN-193189 (ALK2/3 inhibitor); #7, A 83-01 (ALK4/5/7 inhibitor); #8, SAG 21k (Hedgehog signaling activator); #9, Vismodegib (Hedgehog signaling inhibitor); #10, MHY1485 (mTOR activator); #11, VO-OHpic (PTEN inhibitor, PI3K/mTOR activator); #12, SF1670 (PTEN inhibitor, PI3K/mTOR activator); #13, Rapamycin (mTOR inhibitor); #14, ATRA (RA signaling activator); #15, MK-206 (AKT inhibitor); #16, PD0325901 (MEK inhibitor); #17, PIK-90 (PI3K inhibitor); #18, DAPT (γ-secretase inhibitor, Notch inhibitor).

(C-D) Bulk RNA-seq transcriptome analysis of hPSCs (day 0), LPM (day 2), LBM cells (day 4), ExpLBM cells (passage numbers 4–5), and aggregates treated under the following conditions: (i) 30 ng/mL BMP4 and 10 ng/mL TGFβ1 (condition #0), (ii) 30 ng/mL BMP4, 10 ng/mL TGFβ1, and 10% FBS (condition #1), (iii) 30 ng/mL BMP4, 10 ng/mL TGFβ1, and 500 nM PD-0325901 (condition #16, referred to as IZ/ACP organoid), (iv) 300 ng/mL BMP4, 100 ng/mL TGFβ1, and 10% FBS (condition #2, referred to as GPC organoid). n = 2 biologically independent experiments. Principal component analysis (C) and heatmap of gene expression levels for each marker (D).

(E) Histological analysis of ExpLBM aggregates, IZ/ACP organoid, and GPC organoid was performed using haematoxylin–eosin (HE), Alcian blue, or Safranin O staining, and immunohistological analysis with antibodies against SOX9, ACAN, COL1, COL2, COLX, PRG4, RUNX2, and SP7.

(F) UMAP embedding of scRNA-seq data from ExpLBM cells (9741 cells), IZ/ACP organoid (5090 cells), and GPC organoid (4660 cells). UMAP clustering identified 6 clusters, including limb-bud mesenchymal cells (non-dividing) and MKI67+ limb-bud mesenchymal cells (dividing) in ExpLBM cells; GDF5-positive interzone cells and PRG4-positive articular chondrocyte progenitor cells in IZ/ACP organoid; and IHH-positive pre-hypertrophic chondrocytes and SP7-positive hypertrophic chondrocytes in GPC organoid.

(G) Feature plots for each marker gene in the UMAP of integrated scRNA-seq datasets from

ExpLBM cells, IZ/ACP organoid, and GPC organoid

(H) UMAP of integrated scRNA-seq profiles of ExpLBM cells, IZ/ACP organoid and GPC organoid with the human embryonic limb cells from PCW 5 to PCW 9 (119870 cells). Cells are colored by origin: human embryonic limb cells (gray), ExpLBM cells(green), IZ/ACP organoid (red) and GPC organoid (blue). The original datasets of the human embryonic limb cells are from the paper Zhang et al [27].

(I) Dot plots showing the expression of cell-type-specific genes in each cluster of scRNA-seq analysis of human embryonic limb cells and expression of scRNA-seq profiles of ExpLBM cells, IZ/ACP organoid and GPC organoid.

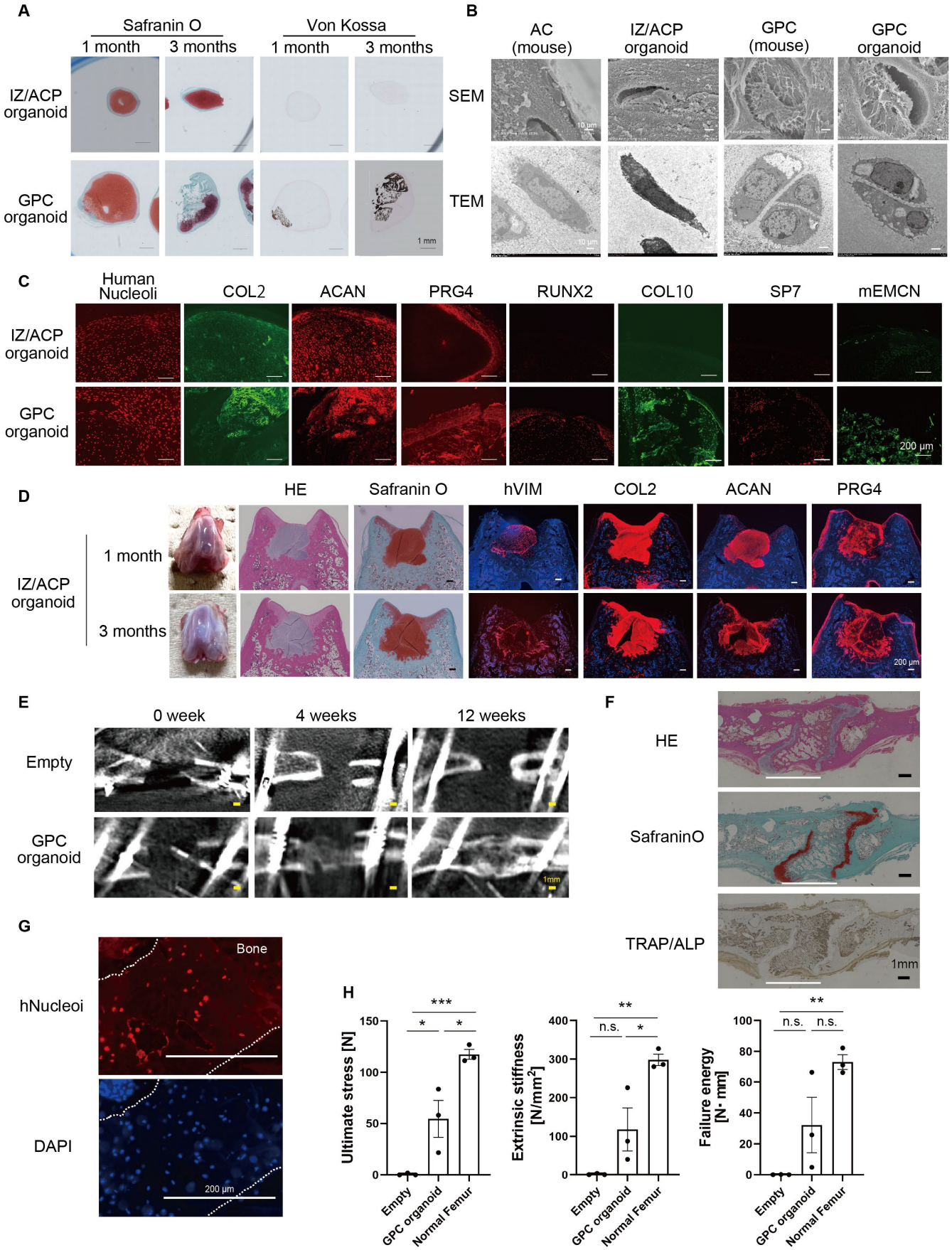
A
Safranin O
Von Kossa
1 month
3 months
1 month
3 months
IZ/ACP organoid
GPC organoid
1 mm
B
AC (mouse)
IZ/ACP organoid
GPC (mouse)
GPC organoid
SEM
TEM
C
Human Nucleoli
COL2
ACAN
PRG4
RUNX2
COL10
SP7
mEMCN
IZ/ACP organoid
GPC organoid
200 µm
D
HE
Safranin O
hVIM
COL2
ACAN
PRG4
IZ/ACP organoid
1 month
3 months
200 µm
E
0 week
4 weeks
12 weeks
Empty
GPC organoid
1mm
F
HE
SafraninO
TRAP/ALP
1mm
G
hNucleoi
DAPI
Bone
200 µm
H
Ultimate stress [N]
Extrinsic stiffness [N/mm²]
Failure energy [N·mm]
Empty
GPC organoid
Normal Femur
***
**
n.s.
*

Figure 2

Figure 2: Assessment of IZ/ACP and GPC organoids on graft fate and regenerative capacity.
(A-C) Subcutaneous transplantation of IZ/ACP or GPC organoids into NOD-SCID mice. Their engraftment was histologically assessed at 12 weeks after transplantation by Safranin O and Von Kossa staining (A), immunohistological analysis (B), and scanning electron microscopy and transmission electron microscopy (C).
(D) Transplantation of ExpLBM-derived IZ/ACP organoid into osteochondral defects of articular cartilage in SCID rats. The knee joints were harvested 1 and 3 months after transplantation. Histological examination was performed on osteochondral defects engrafted with IZ/ACP organoid. At 1 or 3 month post-transplantation, the knee joints were fixed, and tissue sections were stained with Safranin O or with antibodies against human VIMENTIN, COL2, ACAN, or PRG4. Representative images are displayed.
(E) Engraftment of GPC organoid into critical-sized femoral defects in SCID rats was assessed at 4 or 12 week post-transplantation using μCT image analysis.
(F-G) Engraftment of GPC organoid into critical-sized femoral defects in SCID rats was histologically assessed eight weeks post-transplantation using H&E, Safranin O, and ALP/TRAP staining (F), as well as immunostaining with a human-specific nucleoli antibody (G).
(H) Bone strength in critical-sized femoral defects was assessed 12 weeks post-transplantation using a three-point bending test.

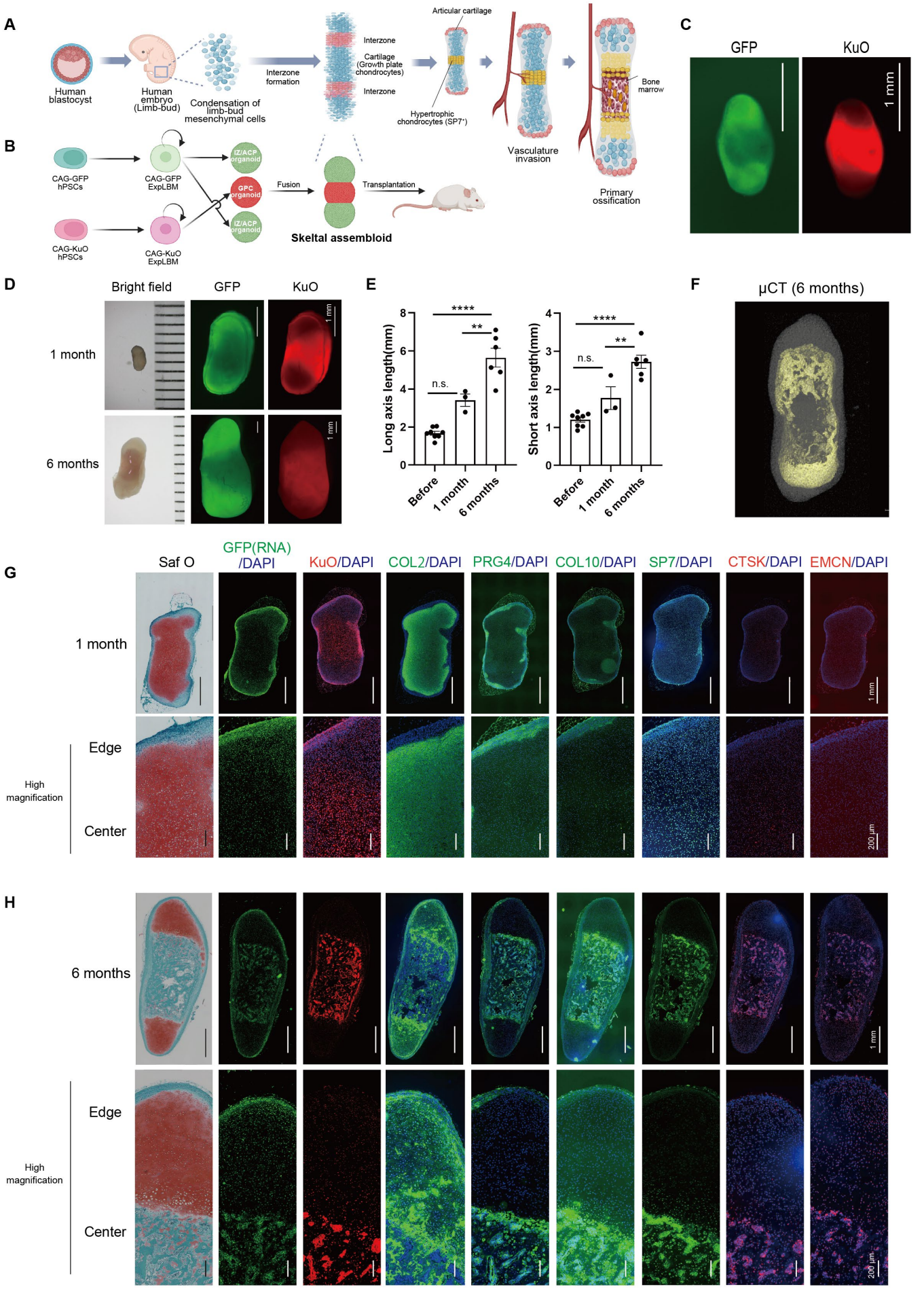
A
Human blastocyst
Human embryo (Limb-bud)
Condensation of limb-bud mesenchymal cells
Interzone formation
Interzone
Cartilage (Growth plate chondrocytes)
Interzone
Articular cartilage
Hypertrophic chondrocytes (SP7+)
Vasculature invasion
Bone marrow
Primary ossification
B
CAG-GFP hPSCs
CAG-GFP ExpLBM
CAG-KuO hPSCs
CAG-KuO ExpLBM
IZ/ACP organoid
GPC organoid
IZ/ACP organoid
Fusion
Skeltal assembloid
Transplantation
C
GFP
KuO
1 mm
D
Bright field
GFP
KuO
1 month
6 months
1 mm
E
Long axis length(mm)
Short axis length(mm)
n.s.
**
****
Before
1 month
6 months
F
μCT (6 months)
G
Saf O
GFP(RNA) /DAPI
KuO/DAPI
COL2/DAPI
PRG4/DAPI
COL10/DAPI
SP7/DAPI
CTSK/DAPI
EMCN/DAPI
1 month
High magnification
Edge
Center
1 mm
200 μm
H
6 months
High magnification
Edge
Center
1 mm
200 μm

Figure 3

Figure 3: Generation of skeletal assembloid with IZ/ACP and GPC organoid to recapitulate human limb skeletal development.

(A) Schematic drawing of skeletal development in the limb. Skeletogenesis begins with limb-bud mesenchymal cell condensation, followed by the formation of skeletal anlagen composed of immature chondrocytes. The joint interzone develops at the position of the presumptive joint and precedes articular cartilage differentiation and joint cavitation. Immature chondrocytes outside the interzone undergo hypertrophy at the mid-diaphysis as the first step of endochondral ossification. Vasculature invades hypertrophic chondrocytes and subsequently forms the bone marrow cavity and growth plate cartilage, which support the growth and elongation of the limbs until puberty, when their closure halts any further skeletal growth.

(B) Graphical illustration of the approach to generate assembloid from GFP-labeled IZ/ACP organoids and KuO-labeled GPC organoids.

(C) Fluorescent images of a typical example of a skeletal assembloid fabricated with KuO-labeled GPC organoid sandwiched with two GFP-labeled IZ/ACP organoids, followed by culture for 7 days.

(D) Subcutaneous transplantation of skeletal assembloid into NOD-SCID mice. Representative bright-field and fluorescent images of assembloid at 1 or 6 months after transplantation.

(E) Long and short length of skeletal assembloid at 1 or 6 months after transplantation.

(F) μCT images of skeletal assembloid at 6 months after transplantation.

(G) The engraftment was histologically assessed at 1 month after transplantation by Safranin O staining and immunohistological analysis.

(H) The engraftment was histologically assessed at 6 months after transplantation by Safranin O staining and immunohistological analysis.

REFERENCES

1. Teti, A. (2011). Bone development: overview of bone cells and signaling. Curr. Osteoporos. Rep. *9*, 264–273.

2. Katz, J.N., Arant, K.R., and Loeser, R.F. (2021). Diagnosis and treatment of hip and knee osteoarthritis: A Review: A review. JAMA *325*, 568–578.

3. Sharma, L. (2021). Osteoarthritis of the knee. N. Engl. J. Med. *384*, 51–59.

4. Calori, G.M., Mazza, E.L., Mazzola, S., Colombo, A., Giardina, F., Romanò, F., and Colombo, M. (2017). Non-unions. Clin. Cases Miner. Bone Metab. *14*, 186–188.

5. Geister, K.A., and Camper, S.A. (2015). Advances in skeletal dysplasia genetics. Annu. Rev. Genomics Hum. Genet. *16*, 199–227.

6. Yamanaka, S. (2020). Pluripotent stem cell-based cell therapy-promise and challenges. Cell Stem Cell *27*, 523–531.

7. Berendsen, A.D., and Olsen, B.R. (2015). Bone development. Bone *80*, 14–18.

8. Long, F. (2011). Building strong bones: molecular regulation of the osteoblast lineage. Nat. Rev. Mol. Cell Biol. *13*, 27–38.

9. Kronenberg, H.M. (2003). Developmental regulation of the growth plate. Nature *423*, 332–336.

10. Ikeda, Y., Tani, S., Moriishi, T., Kuroda, A., Matsuo, Y., Saeki, N., Inui-Yamamoto, C., Abe, M., Maeda, T., Rowe, D.W., et al. (2023). Modeling of intramembranous ossification using human pluripotent stem cell-derived paraxial mesoderm derivatives. Regen Ther *24*, 536–546.

11. Kawai, S., Yoshitomi, H., Sunaga, J., Alev, C., Nagata, S., Nishio, M., Hada, M., Koyama, Y., Uemura, M., Sekiguchi, K., et al. (2019). In vitro bone-like nodules generated from patient-derived iPSCs recapitulate pathological bone phenotypes. Nat Biomed Eng *3*, 558–570.

12. Kidwai, F., Mui, B.W.H., Arora, D., Iqbal, K., Hockaday, M., de Castro Diaz, L.F., Cherman, N., Martin, D., Myneni, V.D., Ahmad, M., et al. (2020). Lineage-specific differentiation of osteogenic progenitors from pluripotent stem cells reveals the FGF1-RUNX2 association in neural crest-derived osteoprogenitors: FGF1 IN NEURAL CREST-DERIVED OSTEOPROGENITORS. Stem Cells *38*, 1107–1123.

13. Xi, H., Fujiwara, W., Gonzalez, K., Jan, M., Liebscher, S., Van Handel, B., Schenke-Layland, K., and Pyle, A.D. (2017). In vivo human somitogenesis guides somite development from hPSCs. Cell Rep. *18*, 1573–1585.

14. Kawai, S., Sunaga, J., Nagata, S., Nishio, M., Fukuda, M., Kamakura, T., Sun, L., Jin, Y., Sakamoto, S., Watanabe, A., et al. (2023). 3D osteogenic differentiation of human iPSCs reveals the role of TGFβ signal in the transition from progenitors to osteoblasts and osteoblasts to osteocytes. Sci. Rep. *13*, 1094.

15. Loh, K.M., Chen, A., Koh, P.W., Deng, T.Z., Sinha, R., Tsai, J.M., Barkal, A.A., Shen, K.Y., Jain, R., Morganti, R.M., et al. (2016). Mapping the Pairwise Choices Leading from Pluripotency to Human Bone, Heart, and Other Mesoderm Cell Types. Cell *166*, 451–467.

16. Wu, C.-L., Dicks, A., Steward, N., Tang, R., Katz, D.B., Choi, Y.-R., and Guilak, F. (2021). Single cell transcriptomic analysis of human pluripotent stem cell chondrogenesis. Nat. Commun. *12*, 362.

17. Umeda, K., Zhao, J., Simmons, P., Stanley, E., Elefanty, A., and Nakayama, N. (2012). Human chondrogenic paraxial mesoderm, directed specification and prospective isolation from pluripotent stem cells. Sci. Rep. *2*, 455.

18. Craft, A.M., Rockel, J.S., Nartiss, Y., Kandel, R.A., Alman, B.A., and Keller, G.M. (2015). Generation of articular chondrocytes from human pluripotent stem cells. Nat. Biotechnol. *33*, 638–645.

19. Pretemer, Y., Kawai, S., Nagata, S., Nishio, M., Watanabe, M., Tamaki, S., Alev, C., Yamanaka, Y., Xue, J.-Y., Wang, Z., et al. (2021). Differentiation of Hypertrophic Chondrocytes from Human iPSCs for the In Vitro Modeling of Chondrodysplasias. Stem Cell Reports *16*, 610–625.

20. Tani, S., Okada, H., Onodera, S., Chijimatsu, R., Seki, M., Suzuki, Y., Xin, X., Rowe, D.W., Saito, T., Tanaka, S., et al. (2023). Stem cell-based modeling and single-cell multiomics reveal gene-regulatory mechanisms underlying human skeletal development. Cell Rep., 112276.

21. Iimori, Y., Morioka, M., Koyamatsu, S., and Tsumaki, N. (2021). Implantation of human-induced pluripotent stem cell-derived cartilage in bone defects of mice. Tissue Eng. Part A *27*, 1355–1367.

22. Smeeton, J., Askary, A., and Crump, J.G. (2017). Building and maintaining joints by exquisite

local control of cell fate. Wiley Interdiscip. Rev. Dev. Biol. *6*. https://doi.org/10.1002/wdev.245.

23. Yamada, D., Nakamura, M., Takao, T., Takihira, S., Yoshida, A., Kawai, S., Miura, A., Ming, L., Yoshitomi, H., Gozu, M., et al. (2021). Induction and expansion of human PRRX1+ limb-bud-like mesenchymal cells from pluripotent stem cells. Nat Biomed Eng *5*, 926–940.

24. Takao, T., Yamada, D., and Takarada, T. (2022). A protocol to induce expandable limb-bud mesenchymal cells from human pluripotent stem cells. STAR Protoc *3*, 101786.

25. Long, H.K., Prescott, S.L., and Wysocka, J. (2016). Ever-changing landscapes: Transcriptional enhancers in development and evolution. Cell *167*, 1170–1187.

26. Klemm, S.L., Shipony, Z., and Greenleaf, W.J. (2019). Chromatin accessibility and the regulatory epigenome. Nat. Rev. Genet. *20*, 207–220.

27. Zhang, B., He, P., Lawrence, J.E.G., Wang, S., Tuck, E., Williams, B.A., Roberts, K., Kleshchevnikov, V., Mamanova, L., Bolt, L., et al. (2023). A human embryonic limb cell atlas resolved in space and time. Nature. https://doi.org/10.1038/s41586-023-06806-x.

28. McQueen, C., and Towers, M. (2020). Establishing the pattern of the vertebrate limb. Development *147*. https://doi.org/10.1242/dev.177956.

29. Baker, C.E., Moore-Lotridge, S.N., Hysong, A.A., Posey, S.L., Robinette, J.P., Blum, D.M., Benvenuti, M.A., Cole, H.A., Egawa, S., Okawa, A., et al. (2018). Bone fracture acute phase response-A unifying theory of fracture repair: Clinical and scientific implications. Clin. Rev. Bone Miner. Metab. *16*, 142–158.

30. Yamashita, A., Morioka, M., Yahara, Y., Okada, M., Kobayashi, T., Kuriyama, S., Matsuda, S., and Tsumaki, N. (2015). Generation of scaffoldless hyaline cartilaginous tissue from human iPSCs. Stem Cell Reports *4*, 404–418.

31. Umeda, K., Oda, H., Yan, Q., Matthias, N., Zhao, J., Davis, B.R., and Nakayama, N. (2015). Long-term expandable SOX9+ chondrogenic ectomesenchymal cells from human pluripotent stem cells. Stem Cell Reports *4*, 712–726.

32. Chen, H., Tan, X.-N., Hu, S., Liu, R.-Q., Peng, L.-H., Li, Y.-M., and Wu, P. (2021). Molecular mechanisms of chondrocyte proliferation and differentiation. Front. Cell Dev. Biol. *9*, 664168.

33. Zhang, Y., Pizzute, T., and Pei, M. (2014). A review of crosstalk between MAPK and Wnt signals and its impact on cartilage regeneration. Cell Tissue Res. *358*, 633–649.

34. Stanton, L.-A., Underhill, T.M., and Beier, F. (2003). MAP kinases in chondrocyte

differentiation. Dev. Biol. *263*, 165–175.

35. Onesto, M.M., Kim, J.-I., and Pasca, S.P. (2024). Assembloid models of cell-cell interaction to study tissue and disease biology. Cell Stem Cell *0*. https://doi.org/10.1016/j.stem.2024.09.017.

36. Aghajanian, P., and Mohan, S. (2018). The art of building bone: emerging role of chondrocyte-to-osteoblast transdifferentiation in endochondral ossification. Bone Res. *6*, 19.

37. Andersen, J., Revah, O., Miura, Y., Thom, N., Amin, N.D., Kelley, K.W., Singh, M., Chen, X., Thete, M.V., Walczak, E.M., et al. (2020). Generation of functional human 3D Cortico-motor assembloids. Cell *183*, 1913-1929.e26.

38. Kim, S.-I., Oceguera-Yanez, F., Sakurai, C., Nakagawa, M., Yamanaka, S., and Woltjen, K. (2016). Inducible transgene expression in human iPS cells using versatile All-in-One piggyBac transposons. Methods Mol. Biol. *1357*, 111–131.

39. Buenrostro, J.D., Giresi, P.G., Zaba, L.C., Chang, H.Y., and Greenleaf, W.J. (2013). Transposition of native chromatin for fast and sensitive epigenomic profiling of open chromatin, DNA-binding proteins and nucleosome position. Nat. Methods *10*, 1213–1218.

40. Hao, Y., Hao, S., Andersen-Nissen, E., Mauck, W.M., 3rd, Zheng, S., Butler, A., Lee, M.J., Wilk, A.J., Darby, C., Zager, M., et al. (2021). Integrated analysis of multimodal single-cell data. Cell *184*, 3573-3587.e29.

41. McGinnis, C.S., Murrow, L.M., and Gartner, Z.J. (2019). DoubletFinder: Doublet detection in single-cell RNA sequencing data using artificial nearest neighbors. Cell Syst. *8*, 329-337.e4.

42. Trapnell, C., Cacchiarelli, D., Grimsby, J., Pokharel, P., Li, S., Morse, M., Lennon, N.J., Livak, K.J., Mikkelsen, T.S., and Rinn, J.L. (2014). The dynamics and regulators of cell fate decisions are revealed by pseudotemporal ordering of single cells. Nat. Biotechnol. *32*, 381–386.